Effect of fluid properties variations on spatio-temporal instability of convection

Sergey A. Suslov

ssuslov@usq.edu.au

Abstract

The classical problem of stability of convection flow in a tall vertical differentially heated rectangular cavity is considered. It is shown that realistic nonlinear fluid properties variations associated with a large cross-cavity temperature gradient lead to significant deviations from the flow scenarios predicted using conventional Boussinesq approximation. It is well known that in the Boussinesq limit of a small temperature gradient the conduction state bifurcates supercritically to a stationary transverse roll pattern associated with the shear of the primary flow, and this instability is of absolute character. Here we show that when the fluid properties vary, a new buoyancy driven oscillatory instability arises, the transition to shear driven instability becomes subcritical, and a range of parameters appears for which the character of instability is convective. Analytical results are obtained by deriving and solving the Ginzburg-Landau-type disturbance amplitude equation and are checked against the results of direct numerical simulation.

1 Introduction and problem definition

Buoyancy driven flow in a two-dimensional vertical rectangular cavity has been the subject of intensive study for the last few decades, see classical works by Rudakov [5] and Bergholz [1] just to name a few. Normally the approach is to use the so-called Boussinesq approximation of the Navier-Stokes equations which assumes no fluid properties variations except a linear density dependence on the temperature in the buoyancy term. As a result the equations are artificially symmetric and the predicted flow solutions are relatively simple. Such an approach is valid only if the maximum temperature difference in the flow region does not exceed a few degrees Kelvin. This limitation is too restrictive for many practical applications such as gas thermal insulation systems and various chemical vapour deposition reactors. In this work the so-called Low-Mach-Number (LMN) equations [2] are used to account for realistic fluid properties variations which lead to diverse flow patterns in comparison to those in the classical Boussinesq flows.

Consider the flow of air with the average (reference) temperature $T_r = 300K$ in a tall closed cavity with isothermal vertical walls separated by a distance H and maintained at different temperatures T_h and T_c, $T_h > T_c$. The density ρ, dynamic

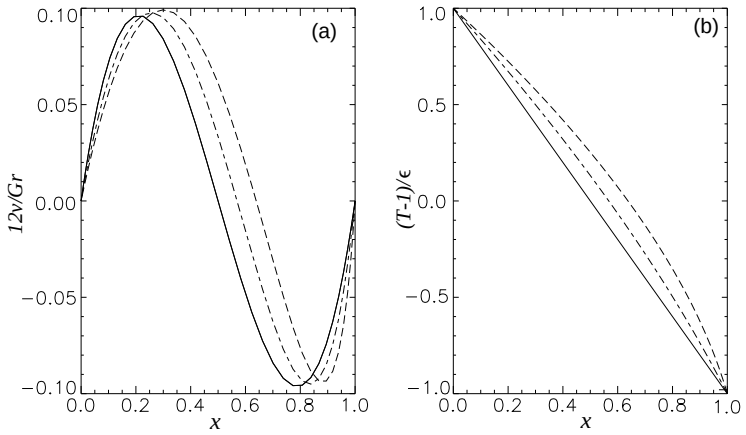

Figure 1: Basic flow velocity (a) and temperature (b) profiles in the Boussinesq ($\epsilon \to 0$, solid line), weakly non-Boussinesq ($\epsilon = 0.3$, dash-dotted line) and strongly non-Boussinesq ($\epsilon = 0.6$, dashed line) regimes.

viscosity μ, thermal conductivity k and specific heat c_p of air are non-dimensionalised with respect to their values at T_r and vary with temperature T and thermodynamic pressure P according to the ideal gas equation of state and Sutherland formulae

$$\rho T = P, \quad \mu = T^{3/2}\frac{1.368}{T+0.368}, \quad k = T^{3/2}\frac{1.648}{T+0.648}, \quad c_p = 1\,. \tag{1}$$

As discussed in [6] such flow is described by LMN equations [2]

$$\rho\left(\tfrac{\partial u_i}{\partial t} + u_j\tfrac{\partial u_i}{\partial x_j}\right) = -\tfrac{\partial \Pi}{\partial x_i} + \tfrac{Gr}{2\epsilon}(\rho-1)n_i + \tfrac{\partial \tau_{ij}}{\partial x_j}\,, \tag{2}$$

$$\rho c_p\left(\tfrac{\partial T}{\partial t} + u_j\tfrac{\partial T}{\partial x_j}\right) = \Gamma\beta T\tfrac{dP}{dt} + \tfrac{1}{Pr}\tfrac{\partial}{\partial x_j}\left(k\tfrac{\partial T}{\partial x_j}\right)\,, \tag{3}$$

$$\tfrac{\partial \rho}{\partial t} + \tfrac{\partial \rho u_j}{\partial x_j} = 0\,. \tag{4}$$

where the Grashof (Gr) and Prandtl (Pr) numbers, the non-dimensional temperature difference (ϵ) between the walls and the measure of fluid resilience (Γ) are defined using the reference values:

$$Gr = \frac{\rho_r^2 g(T_h - T_c)H^3}{\mu_r^2 T_r},\ \epsilon = \frac{T_h - T_c}{2T_r},\ Pr = \frac{\mu_r c_{pr}}{k_r} = 0.71,\ \Gamma = \frac{c_{pr} - c_{vr}}{c_{pr}} = \frac{2}{7}\,.$$

The coefficient of thermal expansion of air is $\beta = 1/T$. Since the cavity is closed and the density of the fluid varies, the nontrivial total mass conservation and zero mass flux conditions,

$$\int_V \rho\,\mathrm{d}V = \text{const.},\ \text{and}\ \int_S \rho v\,\mathrm{d}S = 0\,, \tag{5}$$

are necessary to define a well posed problem.

Figure 1 shows steady parallel basic flow solutions $(v(x), T(x))$ for various values of ϵ. Such flows exist at the relatively small Grashof numbers. The classical Boussinesq cubic velocity and linear temperature profiles exist only in the limit $T_h \to T_c$. See that the property variations associated with any finite cross-cavity temperature gradient break the symmetry of the velocity profile and destroy the linearity of the wall-to-wall conduction temperature profile. The overall effect is that both velocity and temperature gradients steepen near the cold wall. This strongly affects the stability characteristics of the parallel conduction flow regime as will be shown in Section 2. See [6] for more detailed discussion of the basic flow.

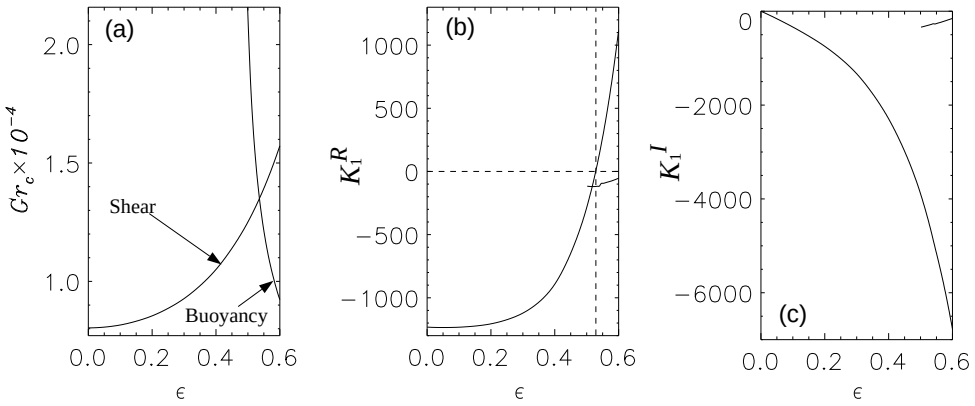

Figure 2: Linear stability diagram (a) and real (b) and imaginary (c) parts of the first Landau constant K_1 as functions of ϵ.

2 Linear and weakly nonlinear stability results

The stability of the parallel flows introduced in Section 1 is investigated in a standard way: the equations are linearized about the basic flow and then the Fourier transform of the resulting equations is taken in a vertical y-direction to form an eigenvalue problem for the disturbance complex amplification rate $\sigma(\alpha)$, where α is the wavenumber in the Fourier transform, see [6] for details. Then by varying Gr for fixed ϵ and α the value $Gr_0(\epsilon, \alpha)$ for which the real part $\sigma^R(\alpha) = 0$ is found. Finally, the critical value $Gr_c(\epsilon) = \min_\alpha(Gr(\epsilon, \alpha))$ is found and this determines the transition from parallel to y-periodic flows. These results are summarized in Figure 2 (a). See that the value of the critical Grashof number increases rapidly with the temperature difference between the walls. The eigenfunction analysis (not shown here) provides an explanation: the disturbance structures are mostly generated near the inflection point of the basic flow velocity profile where the shear of the flow is maximum. For this reason this type of instability is referred to as *shear instability* and is similar to the classical inviscid Helmholtz instability observed in counterflowing liquid layers. As the value of ϵ increases the inflection point moves towards the (cold) wall where the damping of the disturbance is stronger. For this reason a stronger force (larger Gr) driving the disturbance is required for the instability to grow. Such a situation persists up to $\epsilon \approx 0.534$ where stability of the basic parallel flow start deteriorating (observe the rapidly decreasing Gr_c in the right part of Figure 2 a). The eigenfunction analysis shows that this de-stabilisation is caused by a different mechanism: it is due to thermal disturbances developing near the cold wall where the basic flow temperature profile has the largest gradient (see Figure 1 b). This disturbance leads to an overcooled region forming near the cold wall. The thermal conductivity coefficient for air decreases rapidly with the temperature. Because of this the overcooled region becomes self-preserving as its thermal exchange with the surrounding warmer fluid is suppressed due to the lower conductivity. At the same time the fluid density is inversely proportional to its temperature and thus the overcooled region contains heavier fluid which drops down in the gravity field. Such a scenario is referred to as *buoyancy instability*. It is a consequence of nonlinear density variation with temperature and is found only in strongly non-Boussinesq regimes.

Although linear stability analysis is a powerful tool for studying bifurcation phe-

nomena in fluid flows it only provides a *necessary condition* for flow instability. It does not give answers to two important questions: how large can the disturbance amplitude A grow (which is a measure of deviation of the full flow solution after the bifurcation has occured from the undisturbed basic flow computed for the same set of parameters) and is the physical flow actually stable when it is stable according to linear theory? To answer these questions it is necessary to introduce the the so-called weakly nonlinear stability analysis. Its essence is in description of the flow evolution in near critical regimes by deriving and analysing a low dimensional model of such a flow. The model accounts for the dynamics of a narrow wave envelope of the most amplified disturbances. The application of amplitude expansions to non-Boussinesq convection flows in a cavity was discussed in detail in [7]. There, after a rather lengthy derivation involving the recursive solution of equations arising at different orders in disturbance amplitude A, it was shown that up to the third order in amplitude the model is the Landau equation

$$\frac{\mathrm{d}A}{\mathrm{d}t} = \sigma A + K_1 A|A|^2 \,. \tag{6}$$

Here K_1 is the (complex) Landau constant whose numerical value is determined from the appropriate orthogonality condition between the linear eigenfunction and flow corrections found at various orders of A. The Landau equation (6) has a nontrivial equilibrium solution $|A_e|^2 = -\sigma^R/K_1^R$ which exists either when $\sigma^R > 0$ and $K_1^R < 0$ or when $\sigma^R < 0$ and $K_1^R > 0$ (superscript R denotes real part). The former situation corresponds to the linearly unstable flow ($\sigma^R > 0$) and is referred to as supercritical bifurcation: in this case the linear analysis predicts the correct value for the transitional Grashof number Gr_c. The latter situation is referred to as subcritical bifurcation: the flow is linearly stable ($\sigma^R < 0$), i.e. stable with respect to infinitesimal disturbances, but if an initial disturbance amplitude is larger than $|A_e|$ then (6) predicts unbounded growth of the disturbance (in reality they might saturate but at the larger value than the range of validity of the cubic Landau model). Thus the transition from parallel to periodic flow depends on the actual experimental conditions; one can obtain different flow patterns at the same set of governing parameters by simply starting from different initial conditions. Consequently, the sign of the real part of the Landau constant K_1^R determines the character of bifurcation and is a reflection of the flow complexity. Figure 2 (b) shows the strong influence of fluid property variations on the type of bifurcation occuring in the classical convection problem. Since $K_1^R < 0$ for small ϵ (i.e. the bifurcation is supercritical) it confirms the well documented experimental fact [4] that linear theory provides an excellent prediction of the transitional value of $Gr_c \approx 8037$ in the Boussinesq limit. On the other hand at $\epsilon \approx 0.535$ the bifurcation associated with the shear instability mode changes to subcritical and linear theory is not expected to provide a suitable value for Gr_c. Unfortunately, no experiments in this temperature difference range are currently known. Similar analysis of the buoyancy driven instability shows that the corresponding value of K_1^R remains negative predicting supercritical bifurcation for this mode over the whole temperature range considered.

3 Convective and absolute instabilities

The linear and weakly nonlinear analyses of convection presented in Section 2 account for the periodic disturbances corresponding to a single wavenumber α_c at which the maximum temporal disturbance amplification rate $\sigma^R(\alpha_c)$ is observed. This is valid only at the bifurcation point. For any supercritical regime ($Gr > Gr_c$) there is a finite range of wave numbers centered at α_c for which $\sigma^R(\alpha) > 0$, i.e. there exists an envelope of the amplifying disturbance waves all of which will contribute to the asymptotic flow pattern. In order to account for the wave envelope dynamics the Landau model (6) is extended to include weak spatial modulation terms and becomes the Ginzburg-Landau model

$$\frac{\partial A}{\partial t} = \sigma A - (c_g - v)\frac{\partial A}{\partial y} + K_2\frac{\partial^2 A}{\partial y^2} + K_1 A|A|^2\,, \tag{7}$$

where $c_g = \mathrm{i}\frac{\partial\sigma}{\partial\alpha}$ is the disturbance wave group speed, v is the velocity of the moving reference frame with respect to which we will consider the wave dynamics, and $K_2 = -\frac{\partial^2\sigma}{\partial\alpha^2}$. The derivation and justification of this model is the subject of a full length paper currently being prepared by the author. When all coefficients of equation (7) are evaluated at α_c where σ^R has a maximum (i.e. $\frac{\partial\sigma^R}{\partial\alpha} = 0$ and $K_2^R = -\frac{\partial^2\sigma^R}{\partial\alpha^2} > 0$ at this point) the linear stability analysis reveals that the trivial solution $A = 0$ becomes unstable and grows exponentially whenever its amplification rate

$$\gamma_v = \sigma^R - \frac{(c_g - v)^2 K_2^R}{4|K_2|^2} \tag{8}$$

is positive. Obviously, the maximum amplification rate $\gamma_m = \sigma^R(\alpha_c)$ is observed in the frame moving with the wave envelope when $v = c_g$. On the other hand all disturbances will decay in a system moving with a velocity much different from c_g. This observation leads to the introduction of the concepts of *absolute* and *convective* instabilities.

These concepts are roughly illustrated by the waves from a stone thrown into water. If the water flow is fast, only downstream waves will be observed (convective instability). In contrast, in a stagnant pond, waves will propagate in all directions and will eventually perturb the complete water surface (absolute instability). Thus when there exists a system of coordinates in which the localized disturbances amplify, i.e. $\gamma_v > 0$ and $\gamma_{v=0} < 0$ then the instability is convective. The disturbances grow only in the direction of wave propagation. If $\gamma_{v=0} > 0$ then the disturbances amplify at *any fixed* spatial location and the instability is absolute. Naturally, the condition $\gamma_{v=0} = 0$ determines the boundary between convective and absolute instability regimes similar to $\sigma^R = 0$ determining the boundary for linear instability. It is easy to conclude from the above discussion that the linear stability boundary always defines transition between stable and convectively unstable regimes, while absolute instability can arise only in linearly supercritical regimes. The exception is the case of stationary disturbances for which $c_g = 0$. In this case the instability is always absolute.

As seen in Figure 3 (c) the disturbance group speed is negative for any finite temperature difference between the walls. This is consistent with the discussion in

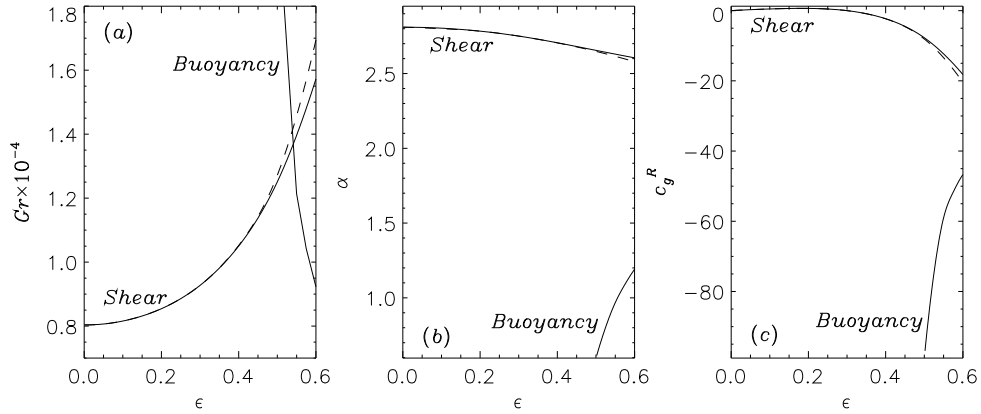

Figure 3: (a) Linear (solid) and absolute (dashed) instability boundaries, (b) corresponding wavenumbers and (c) disturbance wave group speeds as functions of ϵ.

Sections 1 and 2: the shear instability is generated near the inflection point of the basic flow velocity profile, this point moves towards the cold wall where the fluid flows downwards. The buoyancy instability is generated even closer to the cold wall where the basic flow has faster downward velocity. For this reason buoyancy disturbances move downwards substantially faster than shear disturbances.

In the Boussinesq and weakly non-Boussinesq regimes the shear disturbance group speed is close to zero and the difference between the linear and absolute instabilities boundaries cannot be seen in Figure 3 (a) for small values of ϵ, yet it is seen clearly in strongly non-Boussinesq regimes when the symmetry breaking effects of the fluid property variations is more profound. The group speed of the buoyancy disturbances is always so large that a transition to absolute instability for this mode is not found. Note also that the wavelength $2\pi/\alpha$ of the buoyancy disturbance is much larger than that of the shear one, see Figure 3 (b). This emphasises the essentially solitary structure of the buoyancy disturbances (picture them as heavy stones dropping in a surrounding fluid).

To explicitly demonstrate the difference between convective and absolute instability scenarios the Ginzburg-Landau equation (7) is integrated numerically. The coefficients are computed for the supercritical regimes of weakly non-Boussinesq convection with absolute shear driven instability at $\epsilon = 0.3$ and of strongly non-Boussinesq convection with convective buoyancy driven instability at $\epsilon = 0.6$. In a closed cavity the fluid must turn around near the top and bottom ends of the cavity. Consequently, the flow is essentially non-parallel in the end regions which act as a natural source of disturbances for the parallel basic flow existing in the middle part of the cavity. This situation is mimicked by the initial condition for A containing two symmetric pulses near the ends. Since no disturbances are allowed on the solid walls, zero boundary conditions are imposed at $y = 0$ and $y = 40$. In the absolutely unstable regime as depicted in the left part of Figure 4 both initial pulses generate wave packets propagating with the slightly negative group speed from right to left, but the extension rate of each of the envelopes is faster than their translational speed. Eventually both envelopes meet and form a single self-supporting disturbance system extending throughout a complete flow domain. In the convectively unstable regime as shown in the right part of Figure 4 the extension

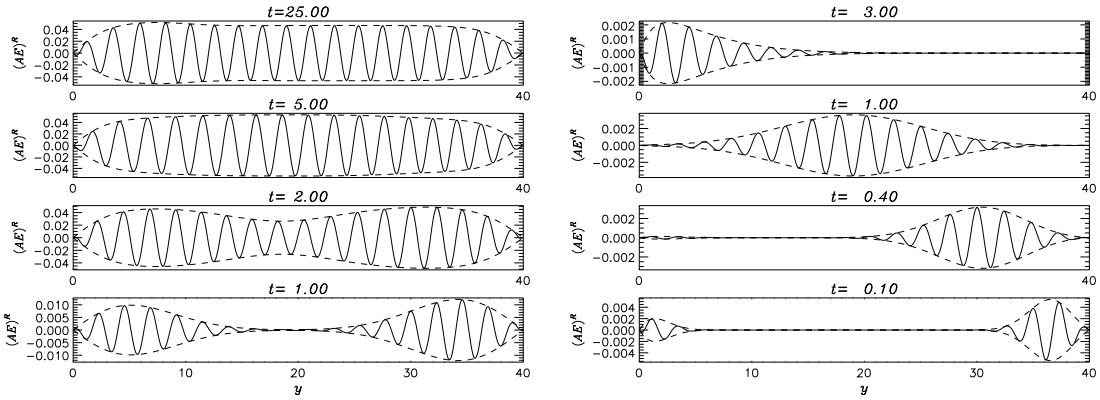

Figure 4: Solutions of equation (7) for $(Gr, \epsilon) = (9860, 0.3)$ (left) and $(Gr, \epsilon) = (16000, 0.6)$ (right).

rate of the wave packets is slower than their translation. For this reason the left envelope is carried quickly towards the wall where it decays due to the absorbing boundary condition. The envelope generated near the right boundary grows as it propagates through the cavity, but eventually hits the left wall and decays as well. Consequently, convectively unstable disturbances can be observed in a closed system only if the flow has a permanent source of external perturbations.

4 Direct numerical simulation and conclusions

Finally, we correlate the conclusions made so far with the results of direct numerical simulation (DNS) of convection in a closed cavity of aspect ratio 40 in the strongly non-Boussinesq regime $(Gr, \epsilon) = (9860, 0.6)$, see Figure 5. Details of a numerical-method are given in [3]. DNS is started from the motionless isothermal state. By time $t = 0.13$ the steady parallel conduction flow is established in the middle part of the cavity. This flow is disturbed by the turning flow in the end regions. In accordance with the analytical conclusions, there is a preferred downward propagation direction for disturbances as seen from the snapshot at $t = 0.53$. Since the considered regime corresponds to the linearly and convectively unstable buoyancy mode, large lumps of cold fluid are seen near the cold wall. Although the shear mode is linearly stable in this regime, its bifurcation is subcritical so that the buoyancy driven disturbances trigger the development of shear instability. The latter is characterised by the shorter wavelength and is clearly seen at $t = 1.22$. Eventually the convectively unstable buoyancy disturbance reaches the bottom wall and dies out while the subcritical shear disturbances continue to determine the flow pattern.

Thus we have demonstrated the strong influence of realistic fluid property variations on all major stability characteristics of the convection flow: from linear stability to bifurcation character to transition between convective and absolute instability regimes and instability mode interaction.

Acknowledgement

This work was partly supported by the USQ Early Researcher Career Grant.

Figure 5: Snapshots of DNS results for thermal (left) and velocity (right) fields at $(Gr, \epsilon) = (9860, 0.6)$. Lighter areas correspond to higher temperature and larger kinetic energy of the fluid, respectively.

References

[1] R.F. Bergholz, *J. Fluid Mech.*, **84**, 743–768, 1978.

[2] D.R. Chenoweth and S. Paolucci, *Phys. Fluids*, **28**, 2365–2374, 1985.

[3] D.R. Chenoweth and S. Paolucci, *J. Fluid Mech.*, **169**, 173–210, 1986

[4] K. Fukui, M. Nakajima, H. Ueda and T. Mizushina, *J. Chem. Engng Japan*, **15**, 172–180, 1982

[5] R.N. Rudakov, *Appl. Math. Mech.*, **31**, 376–383, 1967

[6] S.A. Suslov and S. Paolucci, *Int. J. Heat Mass Transfer*, **38(12)**, 2143–2157, 1995.

[7] S.A. Suslov and S. Paolucci, *J. Fluid Mech.*, **344**, 1–41, 1997.

Dr. Sergey A. Suslov, Department of Mathematics and Computing, University of Southern Queensland, Toowoomba, Queensland 4350, Australia